EUROPEAN ORGANIZATION FOR NUCLEAR RESEARCH (CERN)

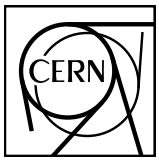

CERN-EP-2022-161
21 July 2022

# Multidifferential study of identified charged hadron distributions in $Z$-tagged jets in proton-proton collisions at $\sqrt{s}$ =13 TeV

**Abstract**

Jet fragmentation functions are measured for the first time in proton-proton collisions for charged pions, kaons, and protons within jets recoiling against a $Z$ boson. The charged-hadron distributions are studied longitudinally and transversely to the jet direction for jets with transverse momentum $20 < p_{\mathrm{T}} < 100$ GeV and in the pseudorapidity range $2.5 < \eta < 4$. The data sample was collected with the LHCb experiment at a center-of-mass energy of 13 TeV, corresponding to an integrated luminosity of 1.64 fb$^{-1}$. Triple differential distributions as a function of the hadron longitudinal momentum fraction, hadron transverse momentum, and jet transverse momentum are also measured for the first time. This helps constrain transverse-momentum-dependent fragmentation functions. Differences in the shapes and magnitudes of the measured distributions for the different hadron species provide insights into the hadronization process for jets predominantly initiated by light quarks.

Submitted to Phys. Rev. D Letter

© 2022 CERN for the benefit of the LHCb collaboration. CC BY 4.0 licence.

Quarks and gluons can never be observed in isolation due to confinement in quantum chromodynamics (QCD). Thus, one of the challenges of QCD lies in relating the quark and gluon degrees of freedom of the theory to the bound-state hadrons observed in nature. A great deal of effort over the past several decades has gone into mapping out nucleon structure in terms of its quark and gluon constituents. A particular focus, in recent years, has been on the three-dimensional imaging of the nucleon [1, 2]. Studying the mechanisms by which colored quarks and gluons hadronize into new color-neutral bound states offers complementary information connecting colored and hadronic degrees of freedom.

In the standard collinear perturbative QCD factorization framework, single-inclusive hadron production in proton-proton ($pp$) collisions factorizes into the short-distance hard scattering of partons and the long-distance dynamics described by fragmentation functions (FFs) and parton distribution functions (PDFs). The latter parametrizes proton structure as a function of momentum fraction carried by a parton of an incoming proton taking part in the hard scattering process. Hadronization of charged particles is described by collinear FFs, denoted as $D_c^h(z)$, where $z$ is the longitudinal momentum fraction of an outgoing parton $c$ carried by a produced hadron $h$ (see Ref. [3] for a review of FFs). The FFs and PDFs are not fully calculable perturbatively and must be constrained by experimental measurements. In Monte Carlo (MC) generators, phenomenological models tuned to data are used to perform hadronization. [4–6]. Jet fragmentation functions (JFFs) are experimental observables describing jet substructure that measure the longitudinal momentum fraction carried by a hadron of a jet [7–13]. Within the soft-collinear effective theory framework, JFFs are constructed such that they can probe the standard collinear FFs, defined for inclusive single-hadron production with no requirement of a reconstructed jet. Similarly, transverse-momentum-dependent (TMD) JFFs defined within the soft-collinear effective theory framework can access standard TMD FFs [14], traditionally measured in $e^+e^-$ collisions [15–18] and semi-inclusive deep inelastic lepton-nucleon scattering [19, 20]. In addition to the dependence on the longitudinal momentum fraction $z$, TMD FFs also depend on $j_{\rm T}$, the transverse momentum of the produced hadron with respect to the jet axis in the case of a fully reconstructed jet, or the thrust axis in $e^+e^-$ collisions (see *e.g.* Ref. [18]). Singly differential TMD JFFs for unidentified hadrons have previously been measured in proton-proton collisions at the LHC [21–24]. The excellent hadron identification capabilities at LHCb allow for measurements of the JFFs for different particle species.

This Letter presents the first measurements of JFFs for identified charged hadrons in jets produced in association with a $Z$ boson in the forward region of $pp$ collisions. The main observables are the longitudinal momentum fraction of the jet carried by the hadron, $z$, and the transverse component of the hadron momentum with respect to the jet axis, $j_{\rm T}$, as found in Ref. [23, 25] and defined as

$$z = \frac{\mathbf{p}_{\rm had} \cdot \mathbf{p}_{\rm jet}}{|\mathbf{p}_{\rm jet}|^2}, \qquad j_{\rm T} = \frac{|\mathbf{p}_{\rm had} \times \mathbf{p}_{\rm jet}|}{|\mathbf{p}_{\rm jet}|}, \tag{1}$$

where $\mathbf{p}_{\rm had}$ and $\mathbf{p}_{\rm jet}$ are the hadron and jet three-momentum vectors, respectively.

The dominant leading order hard process for $Z$+jet production in the LHCb acceptance is $qg \to Zq$ due to the asymmetry between the gluon and quark momentum fractions, verified with Pythia 8 [26], which enhances jets initiated by light valence quarks and provides sensitivity to the quark TMD FFs.

The JFFs measured using $Z$-tagged jets in this Letter are defined in terms of differential

cross-sections $\mathrm{d}\sigma$ as

$$f(z, j_{\mathrm{T}}) = \frac{\mathrm{d}\sigma}{\mathrm{d}\mathcal{PS}\,\mathrm{d}z\,\mathrm{d}j_{\mathrm{T}}} \Big/ \frac{\mathrm{d}\sigma}{\mathrm{d}\mathcal{PS}}, \tag{2}$$

$$F(z) = \int \mathrm{d}j_{\mathrm{T}}\; f(z, j_{\mathrm{T}}) = \frac{\mathrm{d}\sigma}{\mathrm{d}\mathcal{PS}\,\mathrm{d}z} \Big/ \frac{\mathrm{d}\sigma}{\mathrm{d}\mathcal{PS}}, \tag{3}$$

$$F(j_{\mathrm{T}}) = \int \mathrm{d}z\; f(z, j_{\mathrm{T}}) = \frac{\mathrm{d}\sigma}{\mathrm{d}\mathcal{PS}\,\mathrm{d}j_{\mathrm{T}}} \Big/ \frac{\mathrm{d}\sigma}{\mathrm{d}\mathcal{PS}}, \tag{4}$$

where the phase space $\mathrm{d}\mathcal{PS}$ depends on the pseudorapidity of the $Z$ boson and the jet, and the vector sum and the difference between the transverse momenta of the $Z$ boson and the jet [13].

The TMD JFF defined in Eq. (2) is integrated over $j_{\mathrm{T}}$ to obtain the collinear JFF shown in Eq. (3). The transverse profile is obtained by integrating the TMD JFF over $z$ as defined in Eq. (4). Experimentally, these quantities can be expressed in terms of yields corrected for detector effects as

$$f(z, j_{\mathrm{T}}) = \frac{1}{N_{Z+\mathrm{jet}}} \frac{\mathrm{d}N_{\mathrm{had}}(z, j_{\mathrm{T}})}{\mathrm{d}z\,\mathrm{d}j_{\mathrm{T}}},\; F(z) = \frac{1}{N_{Z+\mathrm{jet}}} \frac{\mathrm{d}N_{\mathrm{had}}(z)}{\mathrm{d}z},\; F(j_{\mathrm{T}}) = \frac{1}{N_{Z+\mathrm{jet}}} \frac{\mathrm{d}N_{\mathrm{had}}(j_{\mathrm{T}})}{\mathrm{d}j_{\mathrm{T}}}, \tag{5}$$

where $N_{\mathrm{had}}$ is the number of hadrons in $Z$-tagged jets for given $z$ and $j_{\mathrm{T}}$, and $N_{Z+\mathrm{jet}}$ is the number of $Z$ + jet pairs that contain charged hadrons.

The LHCb detector [27,28] is a single-arm forward spectrometer covering the pseudorapidity range $2 < \eta < 5$. The detector includes a high-precision tracking system consisting of a silicon-strip vertex detector (VELO) [29] surrounding the $pp$ interaction region, a silicon-strip detector located upstream of a dipole magnet with a bending power of about 4 Tm, and three stations of silicon-strip detectors and straw drift tubes [30, 31] placed downstream of the magnet. The momentum resolution of charged particles provided by the tracking system is $\delta p/p \sim 0.5\%$ at low momentum and reaches 1.0% at 200 GeV[1]. The VELO allows reconstruction of multiple primary vertices (PVs) and rejection of events with more than one PV or additional low-momentum tracks. Muons are identified by a system composed of alternating layers of iron and multiwire proportional chambers [32]. Photons, electrons, and hadrons are distinguished by a calorimeter system consisting of scintillating-pad and preshower detectors, an electromagnetic calorimeter, and a hadronic calorimeter. Different types of charged hadrons are identified using information from two ring-imaging Cherenkov (RICH) detectors [33], with RICH 1 ($C_4F_{10}$ radiator) covering momenta 2 to 60 GeV and RICH 2 ($CF_4$) covering 15 to 100 GeV. Simulated $pp$ collisions are generated using Pythia 8 [26] with a specific LHCb configuration [34]. Decays of hadronic particles are described by EvtGen [35], in which final-state radiation is generated using Photos [36]. Finally, the Geant4 toolkit [37] is used to simulate the interactions of the particles with the detector, as described in Ref. [38].

The data sample used in this analysis corresponds to an integrated luminosity of 1.64 fb$^{-1}$ collected at $\sqrt{s} = 13$ TeV with the LHCb detector in 2016. The online event selection is performed by the muon trigger system, where $Z$ boson candidates are selected via their decay into two oppositely charged muons. The two muons are required to have $p_{\mathrm{T}} > 20$ GeV, $2.0 < \eta(\mu) < 4.5$, and their invariant mass within the range

[1]In this article, natural units ($c = \hbar = 1$) are used.

$60 < M_{\mu\mu} < 120$ GeV, as applied in Ref. [23, 39]. The muons must satisfy the track-reconstruction and muon-identification criteria applied in Ref. [40]. Jet reconstruction is performed offline using a particle-flow algorithm [39], where the neutral and charged candidates are clustered using the anti-$k_T$ algorithm [41] as implemented in the FastJet package [42] with a distance parameter $R$ of 0.5. The selection criteria for $Z$+jet pairs and tracks inside the jets closely follow those described in Ref. [23]. The fiducial criteria require that the jet with the highest $p_{\rm T}$ in the event, which is analyzed for these measurements, has $20 < p_{\rm T}(\text{jet}) < 100$ GeV and $2.5 < \eta(\text{jet}) < 4.0$. Additional jets with $p_{\rm T}(\text{jet}) > 15$ GeV are used in unfolding detector effects. The tighter $\eta$(jet) requirement ensures that all the jet constituents are contained within the detector acceptance. To reduce the rate of jets associated with a different primary vertex than the $Z$ candidate, only events with a single reconstructed primary vertex are analyzed. The jets must be well separated from the $Z$ candidate by requiring an azimuthal separation greater than $\frac{7\pi}{8}$, and are rejected if one of the muons is found within $\Delta R = \sqrt{\Delta\eta^2 + \Delta\phi^2} < 0.5$, defined with respect to the jet momentum. The charged hadron candidates must be constituents of the jet, fall within $\Delta R < 0.5$ of the jet, and have a good quality track with a minimum $p_{\rm T}$ ($p$) of 0.25 (4) GeV.

The number of $Z$+jet pairs in each jet $p_{\rm T}$ interval, used in the normalization of the JFFs, is corrected to account for reconstruction and selection efficiencies. The same correction factors are applied to the hadron distributions in jets. The muon detection and reconstruction efficiencies are determined in data using the tag-and-probe method employed in the inclusive $Z$ boson cross-section measurements of LHCb [40, 43, 44]. The efficiency to reconstruct and identify the jet in the event is evaluated from simulation. This efficiency increases with $p_{\rm T}$, from $\approx 85\%$ for jets with $p_{\rm T}$ of 20 GeV to saturate at $\approx 95\%$ for jets with $p_{\rm T}$ of 30 GeV and above.

The charged hadron candidates inside the reconstructed jets are identified by the particle-identification systems [27, 33]. Reconstructed charged hadron yields are corrected for the track-reconstruction efficiency, effects from misreconstructed tracks or false association with jets, and particle misidentification on a track-by-track basis. Simulation is used to determine the track reconstruction efficiency for pions, kaons, and protons separately as a function of momentum and pseudorapidity. The probability of hadronic interactions in the detector material of $\approx$20% $\lambda$ (nuclear interaction lengths), and decays in flight, results in track reconstruction efficiencies of 79%, 77% and 63% for pions, kaons, and protons, respectively.

The particle identification (PID) efficiency is determined in intervals of particle momentum, pseudorapidity, and track multiplicity using dedicated data control samples [45]. The (mis)identification probabilities of charged hadrons are derived from these samples and used to construct a PID matrix. The particle misidentification effects are unfolded by solving

$$\mathbf{x}^{\rm rec} = A\,\mathbf{x}^{\rm unf} \tag{6}$$

in each momentum interval. The vector $\mathbf{x}^{\rm unf}$ represents the unfolded yields of the three particles species $\pi^{\pm}$, $K^{\pm}$, and $p^{\pm}$ in a given momentum interval and $\mathbf{x}^{\rm rec}$ the corresponding reconstructed yields at detector level. A matrix element $A_{\,ij}$ represents the probability of a particle $j$ to be reconstructed as $i$. The probabilities are weighted to describe the pseudorapidity and track-multiplicity distributions in data.

The uncertainties on the resulting PID-unfolded momentum distributions $\mathbf{x}^{\rm unf}$ are

estimated using a bootstrap method [46] with 500 trials and are statistically dominated. The impurity of the charged-hadron sample due to misidentification of nonhadronic particles or long-lived hyperons as charged pions, kaons, or protons is less than 5% of the statistical uncertainties in all momentum intervals. The particle-species-dependent efficiencies can be biased if a particle is misidentified. The efficiencies are corrected for these effects after the PID unfolding.

The unfolding of detector effects in the distributions of transverse momentum and pesudorapidity of jets in $Z$+jet pairs is performed using machine learning (ML) techniques based on the iterative unbinned Bayesian unfolding method as implemented in Ref. [47]. In this method, deep neural networks are employed as classifiers to estimate likelihood ratios that are used to update event weights in simulation. The unfolding method is validated with a closure test using the simulated data. In this analysis, two iterations are performed based on the best results of the closure tests. The unfolded jet-$p_{\mathrm{T}}$ distributions are consistent within statistical uncertainties between the ML method employed in this analysis and the binned iterative Bayesian method [48, 49] with two iterations. The charged hadron distributions inside jets in $z$, $j_{\mathrm{T}}$, and their joint distributions, are unfolded simultaneously with the jet transverse momentum and pseudorapidity.

Sources of systematic uncertainties on the jet transverse-momentum distribution of $Z$+jet pairs and identified charged hadrons in $z$ and $j_{\mathrm{T}}$ are evaluated. The former arise from the background contributions from fake jets (0.2%) and incorrectly reconstructed $Z$ bosons (1.4%) due to hadrons misidentified as muons. Additionally, uncertainties on the jet reconstruction are determined by comparing jet-quality quantifiers between the data and simulation (1.8%), similar to the method employed in Ref. [50]. Uncertainties related to the muon reconstruction efficiencies are found to be negligible. The $Z$+jet selection and jet reconstruction uncertainties added in quadrature return a total uncertainty of 2.4%.

The primary uncertainties associated with the simulated detector response of the jets arise from the jet-energy scale and resolution. The jet-energy scale has been studied in previous measurements of the $Z$+jet cross-section [39, 50]. Exploiting the $p_{\mathrm{T}}$ balance between the $Z$ boson and a single recoiled jet in the event, the uncertainty on the jet-energy scale is determined to be 3%. The uncertainties on the fragmentation measurements are estimated by repeating the analysis with the energy scale in the simulation varied by one standard deviation and taking the difference in the distributions, as in Refs. [23, 39, 50]. Similarly, the systematic uncertainty due to the jet-energy resolution is evaluated by independently varying each component of the reconstructed jet momentum in the simulation by the uncertainty on the jet resolution. This procedure is repeated until the difference in the unfolded distributions between the nominal and smeared jet momentum stabilizes.

The sources of systematic uncertainties on the identified charged-hadron distributions include the tracking efficiency and particle identification. The effects of the statistical precision of the efficiency are evaluated by smoothing the two-dimensional efficiency and repeating the analysis. The differences in the distributions between the smoothed and nominal efficiencies are taken as uncertainties on the tracking efficiency. Additionally, PID-dependent uncertainties attributed to the uncertainties on the material budget implemented in the simulation are found to be 1.50%, 1.27% and 3.3% for pions, kaons, and protons, respectively. The uncertainty on the track-selection requirement to remove spurious tracks formed by accidentally matched detector hits and charged hadrons not

associated with the jet is negligible. For identified charged-hadron distributions, the systematic uncertainties on the PID are determined from the uncertainties on the PID-unfolded momentum distributions.

The systematic uncertainties on the unfolding method are determined by taking the standard deviation of weighted absolute differences in the ratio between the unfolded and generated distributions. The uncertainties on the unfolded number of jets and the non-normalized hadronization variables are 1.1% and 0.8%, respectively.

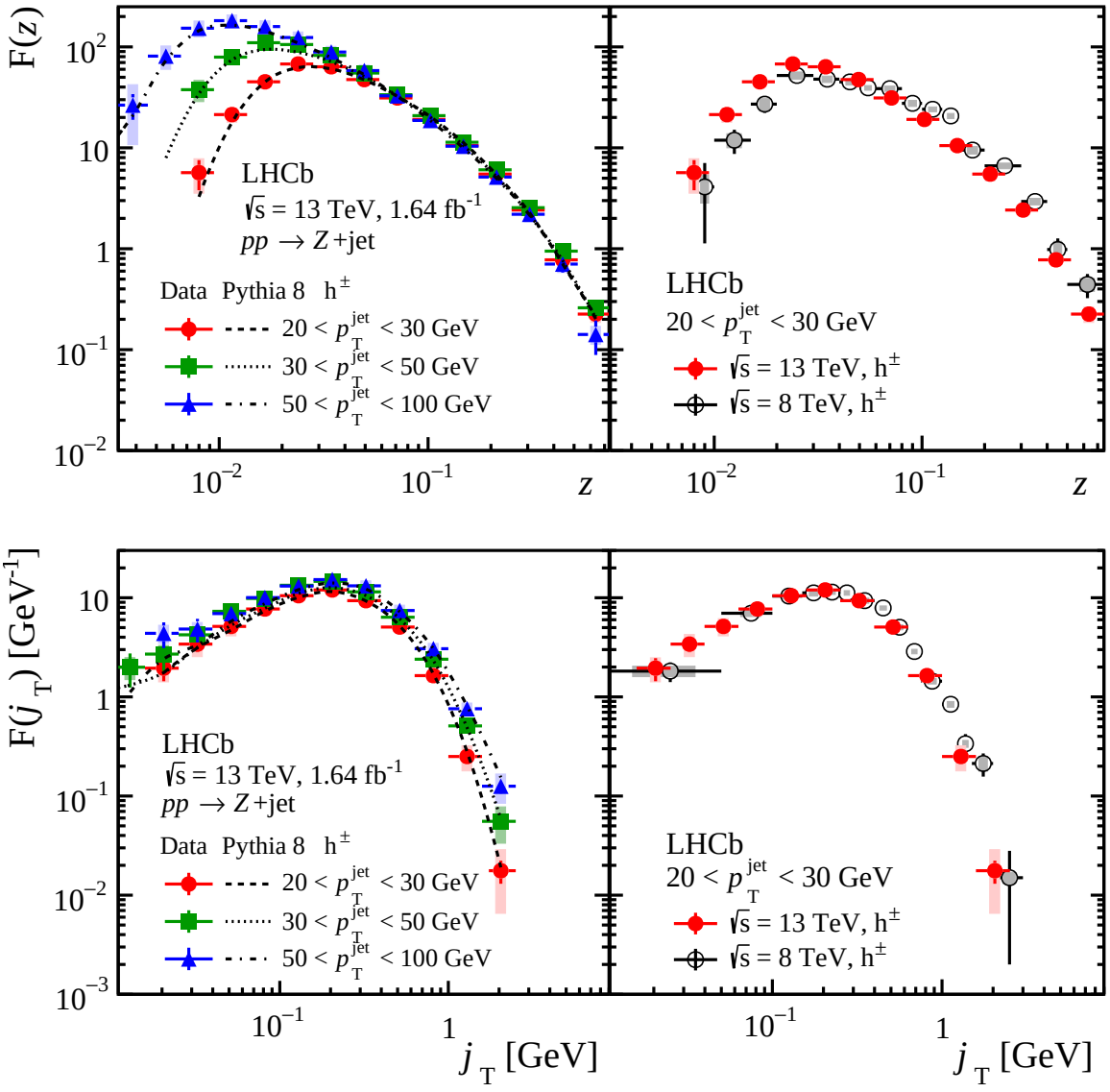


Figure 1: Distributions of (top) the longitudinal momentum fraction and (bottom) the transverse momentum of charged hadrons (pions, kaons, and protons combined) with respect to the jet axis in three jet $p_{\rm T}$ intervals and (right) comparisons with previous results at $\sqrt{s} = 8$ TeV for jets with $20 < p_{\rm T} < 30$ GeV [23]. Statistical (systematic) uncertainties are shown in bars (boxes).

Figure 1 shows $z$ and $j_{\rm T}$ distributions in three intervals of jet $p_{\rm T}$ for unidentified charged hadrons. The $z$ distributions show a humpbacked structure in $z < 0.04$ due to both color coherence and kinematic requirements. Color coherence is a manifestation

of parton hadron duality [51] where the perturbative partonic structure of a jet defines the momenta of the final hadrons, and produces this structure due to the suppression of wide-angle gluon emissions. In these distributions the kinematic requirements on the tracks shift the peak of the structure to varying degrees for different jet $p_{\mathrm{T}}$ intervals; higher $p_{\mathrm{T}}$ jets can probe smaller $z$. At mid-to-high $z$, $0.04 < z < 0.4$, scaling behavior is seen across all jet $p_{\mathrm{T}}$ intervals. An overall increase of particle production in all regions of $j_{\mathrm{T}}$ for jets with higher $p_{\mathrm{T}}$ is seen, with a larger increase at high $j_{\mathrm{T}}$. Comparisons with previous measurements at $\sqrt{s} = 8$ TeV [23] show a general similarity in shape. While the measurements indicate that charged hadron production may be slightly shifted towards lower $z$ at $\sqrt{s} = 13$ TeV for a given jet $p_{\mathrm{T}}$, the $j_{\mathrm{T}}$ distributions are consistent within uncertainties between the two center-of-mass energies.

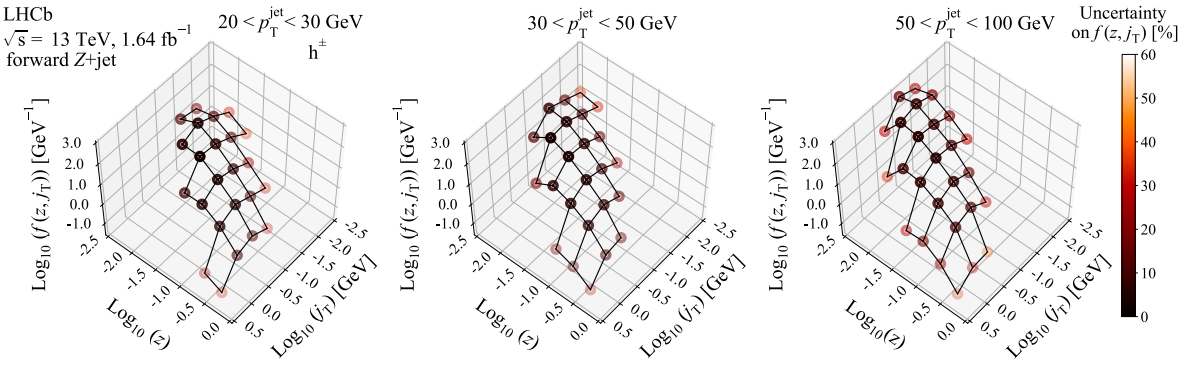


Figure 2: Double differential JFFs of the longitudinal momentum fraction $z$ and the transverse momentum $j_{\mathrm{T}}$ of charged hadrons (pions, kaons, and protons combined) in three jet $p_{\mathrm{T}}$ intervals.

The double differential JFFs in $j_{\mathrm{T}}$, $z$, in three jet $p_{\mathrm{T}}$ intervals for unidentified charged hadrons are shown in Fig. 2. Charged hadrons carrying a larger momentum fraction along the jet axis tend to have a larger transverse momentum with respect to the jet axis. With increasing jet $p_{\mathrm{T}}$, the centroid of the joint distributions moves towards a smaller $z$, a region dominated by soft particle production, and a larger $j_{\mathrm{T}}$, resulting in wider jets. Charged particles also carry a larger $j_{\mathrm{T}}$ for a given $z$ in jets with a higher $p_{\mathrm{T}}$. This is consistent with Markov chain fragmentation models, *e.g.* the string or cluster model, where a momentum kick transverse to the parton system is sampled independently per hadron. Jets with higher $p_{\mathrm{T}}$ experience longer Markov chains, resulting in a higher $j_{\mathrm{T}}$ for a given $z$.

The $z$ distributions for identified charged hadrons and the ratios of heavier particles with respect to pions are shown in Fig. 3. Pions are the predominant charged hadron produced due to their low mass and the flavor content of the initial-state protons. Hadrons with heavier mass require a larger $z$ threshold for their formation, leading to the position of the maximum at a higher $z$. In the lowest jet $p_{\mathrm{T}}$ interval, proton production relative to kaon production is clearly suppressed for lower $z$ values. When different jet $p_{\mathrm{T}}$ intervals are overlaid, the scaling behavior across all jet $p_{\mathrm{T}}$ intervals begins at $z \sim 0.07$ for heavier particles and 0.03 for pions.

The JFFs and the ratios are compared to predictions from Pythia 8 in Fig. 1 and Fig. 3. The predictions are generated using Pythia 8.186 with the CT09MCS PDF

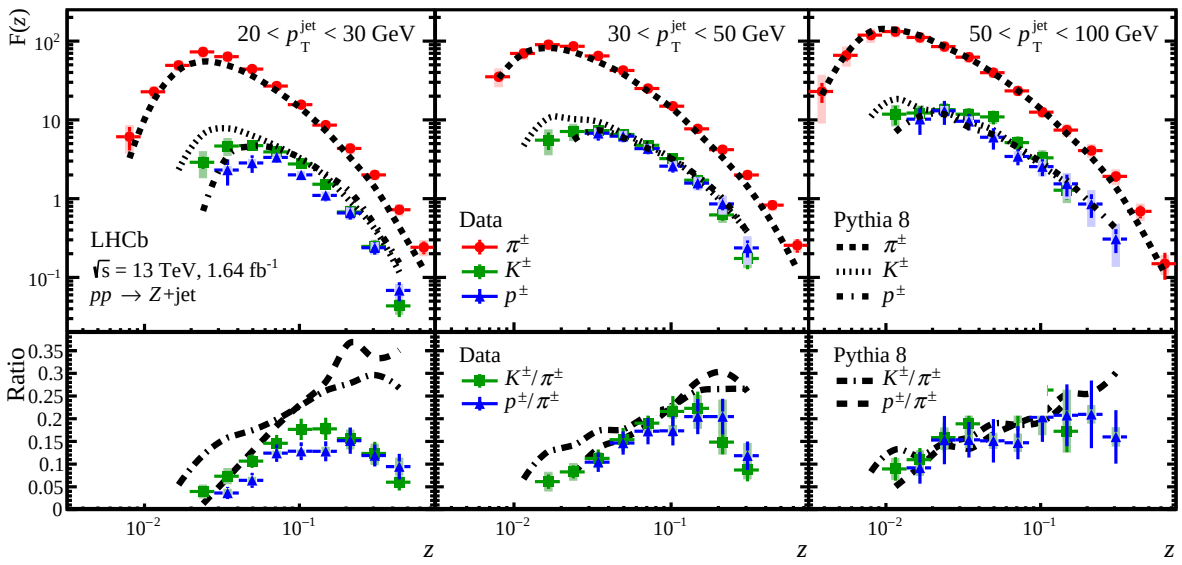


Figure 3: Collinear jet fragmentation functions of (top) identified pions, kaons and protons in three jet $p_T$ intervals and (bottom) the ratios of kaons to pions and protons to pions. Statistical (systematic) uncertainties are shown in bars (boxes).

set and a specific LHCb configuration [34]. In general, PYTHIA 8 describes unidentified charged hadron distributions well with only slight underestimation while the number of charged pions (kaons and protons) are largely underestimated (overestimated). The production of heavier particles relative to pions is well described by PYTHIA 8 at high jet $p_T$, while at low jet $p_T$ PYTHIA 8 significantly overestimates it. These data can be used to tune MC generators for production of identified charged particles.

Figure 4 shows the TMD JFFs measured as joint distributions in $z$ and $j_T$ for the three separate particle species. The center of the distribution shifting towards higher values in both $z$ and $j_T$ with the mass of the particle suggests that heavier hadrons are produced from harder partons.

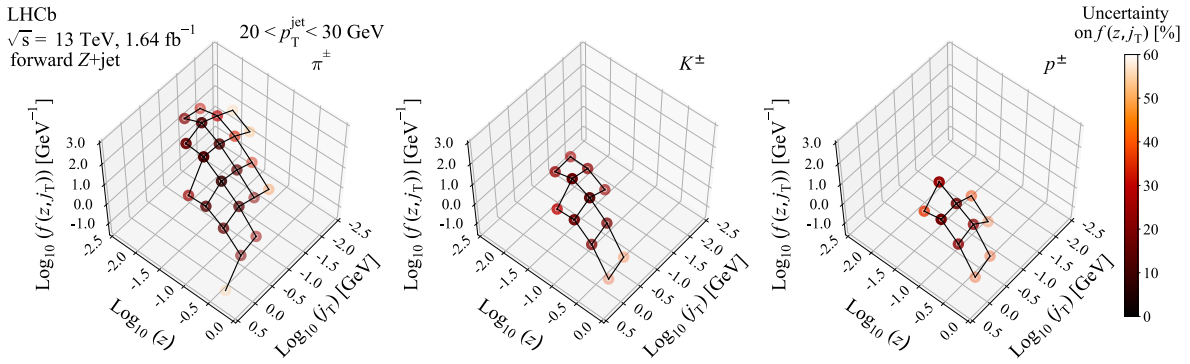


Figure 4: Joint distributions of the longitudinal momentum fraction $z$ and the transverse momentum $j_T$ of identified charged (left) pions, (middle) kaons and (right) protons in jets with $20 < p_T < 30$ GeV.

In summary, the LHCb collaboration has measured the joint distributions in two kinematic variables simultaneously, probing the longitudinal and transverse profiles of identified charged pions, kaons, and protons inside predominantly light-quark-initiated jets for the first time. These distributions describe the 3D picture in the collinear and transverse dimension with respect to the jet axis, and the hadron-mass hierarchy in the hadronization processes. They will help constrain TMD FFs in uncharted phase space. These measurements exploit the full particle-identification capabilities of the LHCb detector. The joint distributions for all charged hadrons have also been measured for the first time.

The collinear JFFs for identified charged hadrons exhibit the effects of quark-flavor content inside the proton. The relative jet-fragmentation functions of heavier particles to pions could provide insights into the role of the valence versus sea quarks in the parton shower leading to hadronization. The projected single-variable distributions in $j_{\mathrm{T}}$ and $z$ have been measured for identified and all charged hadrons and compared to the previous LHCb results at 8 TeV. Overall, similar patterns are seen in $j_{\mathrm{T}}$ and $z > 0.04$ between $\sqrt{s} = 8$ TeV and 13 TeV.

# References


[1] M. Anselmino, A. Mukherjee, and A. Vossen, *Transverse spin effects in hard semi-inclusive collisions*, Prog. Part. Nucl. Phys. **114** (2020) 103806, arXiv:2001.05415.

[2] K. Kumericki, S. Liuti, and H. Moutarde, *GPD phenomenology and DVCS fitting: Entering the high-precision era*, Eur. Phys. J. A **52** (2016) 157, arXiv:1602.02763.

[3] A. Metz and A. Vossen, *Parton fragmentation functions*, Prog. Part. Nucl. Phys. **91** (2016) 136, arXiv:1607.02521.

[4] X. Artru and G. Mennessier, *String model and multiproduction*, Nucl. Phys. B **70** (1974) 93.

[5] B. Andersson, G. Gustafson, G. Ingelman, and T. Sjostrand, *Parton fragmentation and string dynamics*, Phys. Rept. **97** (1983) 31.

[6] G. C. Fox and S. Wolfram, *A model for parton showers in QCD*, Nucl. Phys. B **168** (1980) 285.

[7] M. Procura and I. W. Stewart, *Quark fragmentation within an identified jet*, Phys. Rev. D **81** (2010) 074009, Erratum ibid. **D83** (2011) 039902, arXiv:0911.4980.

[8] T. Kaufmann, A. Mukherjee, and W. Vogelsang, *Hadron fragmentation inside jets in hadronic collisions*, Phys. Rev. D **92** (2015) 054015, Erratum ibid. **D101** (2020) 079901, arXiv:1506.01415.

[9] Y.-T. Chien *et al.*, *Jet fragmentation functions in proton-proton collisions using soft-collinear effective theory*, JHEP **05** (2016) 125, arXiv:1512.06851.

[10] D. Neill, I. Scimemi, and W. J. Waalewijn, *Jet axes and universal transverse-momentum-dependent fragmentation*, JHEP **04** (2017) 020, arXiv:1612.04817.

[11] Z.-B. Kang, F. Ringer, and I. Vitev, *Jet substructure using semi-inclusive jet functions in SCET*, JHEP **11** (2016) 155, arXiv:1606.07063.

[12] Z.-B. Kang, X. Liu, F. Ringer, and H. Xing, *The transverse momentum distribution of hadrons within jets*, JHEP **11** (2017) 068, arXiv:1705.08443.

[13] Z.-B. Kang, K. Lee, J. Terry, and H. Xing, *Jet fragmentation functions for Z-tagged jets*, Phys. Lett. B **798** (2019) 134978, arXiv:1906.07187.

[14] J. Collins, *Foundations of perturbative QCD*, vol. 32, Cambridge University Press, 2013.

[15] Belle collaboration, K. Abe *et al.*, *Measurement of azimuthal asymmetries in inclusive production of hadron pairs in $e^+e^-$ annihilation at Belle*, Phys. Rev. Lett. **96** (2006) 232002, arXiv:hep-ex/0507063.

[16] Belle collaboration, R. Seidl *et al.*, *Measurement of azimuthal asymmetries in inclusive production of hadron pairs in $e^+e^-$ annihilation at $\sqrt{s} = 10.58$ GeV*, Phys. Rev. D **78** (2008) 032011, Erratum ibid. **D86** (2012) 039905, arXiv:0805.2975.

[17] BaBar collaboration, J. P. Lees *et al.*, *Measurement of Collins asymmetries in inclusive production of charged pion pairs in $e^+e^-$ annihilation at BABAR*, Phys. Rev. D **90** (2014) 052003, arXiv:1309.5278.

[18] Belle collaboration, R. Seidl *et al.*, *Transverse momentum dependent production cross sections of charged pions, kaons and protons produced in inclusive $e^+e^-$ annihilation at $\sqrt{s} = 10.58$ GeV*, Phys. Rev. D **99** (2019) 112006, arXiv:1902.01552.

[19] HERMES collaboration, A. Airapetian *et al.*, *Multiplicities of charged pions and kaons from semi-inclusive deep-inelastic scattering by the proton and the deuteron*, Phys. Rev. D **87** (2013) 074029, arXiv:1212.5407.

[20] COMPASS collaboration, M. Aghasyan *et al.*, *Transverse-momentum-dependent multiplicities of charged hadrons in muon-deuteron deep inelastic scattering*, Phys. Rev. D **97** (2018) 032006, arXiv:1709.07374.

[21] ATLAS collaboration, G. Aad *et al.*, *Measurement of the jet fragmentation function and transverse profile in proton-proton collisions at a center-of-mass energy of 7 TeV with the ATLAS detector*, Eur. Phys. J. C **71** (2011) 1795, arXiv:1109.5816.

[22] ATLAS collaboration, G. Aad *et al.*, *Properties of jet fragmentation using charged particles measured with the ATLAS detector in pp collisions at $\sqrt{s} = 13$ TeV*, Phys. Rev. D **100** (2019) 052011, arXiv:1906.09254.

[23] LHCb collaboration, R. Aaij *et al.*, *Measurement of charged hadron production in Z-tagged jets in proton-proton collisions at $\sqrt{s} = 8$ TeV*, Phys. Rev. Lett. **123** (2019) 232001, arXiv:1904.08878.

[24] ALICE collaboration, S. Acharya *et al.*, *Jet fragmentation transverse momentum distributions in pp and p-Pb collisions at $\sqrt{s}$, $\sqrt{s_{\rm NN}} = 5.02$ TeV*, JHEP **09** (2021) 211, arXiv:2011.05904.

[25] STAR collaboration, L. Adamczyk *et al.*, *Azimuthal transverse single-spin asymmetries of inclusive jets and charged pions within jets from polarized-proton collisions at* $\sqrt{s} = 500$ *GeV*, Phys. Rev. D **97** (2018) 032004, arXiv:1708.07080.

[26] T. Sjöstrand, S. Mrenna, and P. Skands, *A brief introduction to PYTHIA 8.1*, Comput. Phys. Commun. **178** (2008) 852, arXiv:0710.3820; T. Sjöstrand, S. Mrenna, and P. Skands, *PYTHIA 6.4 physics and manual*, JHEP **05** (2006) 026, arXiv:hep-ph/0603175.

[27] LHCb collaboration, A. A. Alves Jr. *et al.*, *The LHCb detector at the LHC*, JINST **3** (2008) S08005.

[28] LHCb collaboration, R. Aaij *et al.*, *LHCb detector performance*, Int. J. Mod. Phys. **A30** (2015) 1530022, arXiv:1412.6352.

[29] R. Aaij *et al.*, *Performance of the LHCb Vertex Locator*, JINST **9** (2014) P09007, arXiv:1405.7808.

[30] R. Arink *et al.*, *Performance of the LHCb Outer Tracker*, JINST **9** (2014) P01002, arXiv:1311.3893.

[31] P. d'Argent *et al.*, *Improved performance of the LHCb Outer Tracker in LHC Run 2*, JINST **12** (2017) P11016, arXiv:1708.00819.

[32] A. A. Alves Jr. *et al.*, *Performance of the LHCb muon system*, JINST **8** (2013) P02022, arXiv:1211.1346.

[33] M. Adinolfi *et al.*, *Performance of the LHCb RICH detector at the LHC*, Eur. Phys. J. **C73** (2013) 2431, arXiv:1211.6759.

[34] I. Belyaev *et al.*, *Handling of the generation of primary events in Gauss, the LHCb simulation framework*, J. Phys. Conf. Ser. **331** (2011) 032047.

[35] D. J. Lange, *The EvtGen particle decay simulation package*, Nucl. Instrum. Meth. **A462** (2001) 152.

[36] N. Davidson, T. Przedzinski, and Z. Was, *PHOTOS interface in C++: Technical and physics documentation*, Comp. Phys. Comm. **199** (2016) 86, arXiv:1011.0937.

[37] Geant4 collaboration, S. Agostinelli *et al.*, *Geant4: A simulation toolkit*, Nucl. Instrum. Meth. **A506** (2003) 250; Geant4 collaboration, J. Allison *et al.*, *Geant4 developments and applications*, IEEE Trans. Nucl. Sci. **53** (2006) 270.

[38] M. Clemencic *et al.*, *The LHCb simulation application, Gauss: Design, evolution and experience*, J. Phys. Conf. Ser. **331** (2011) 032023.

[39] LHCb collaboration, R. Aaij *et al.*, *Study of forward Z+jet production in pp collisions at* $\sqrt{s} = 7$ *TeV*, JHEP **01** (2014) 033, arXiv:1310.8197.

[40] LHCb collaboration, R. Aaij *et al.*, *Precision measurement of forward Z boson production in proton-proton collisions at* $\sqrt{s} = 13$ *TeV*, JHEP **07** (2022) 026, arXiv:2112.07458.

[41] M. Cacciari, G. P. Salam, and G. Soyez, *The anti-$k_t$ jet clustering algorithm*, JHEP **04** (2008) 063, arXiv:0802.1189.

[42] M. Cacciari, G. P. Salam, and G. Soyez, *FastJet user manual*, Eur. Phys. J. C **72** (2012) 1896, arXiv:1111.6097.

[43] LHCb collaboration, R. Aaij *et al.*, *Measurement of forward $W$ and $Z$ boson production in pp collisions at $\sqrt{s}$ =8 TeV*, JHEP **01** (2016) 155, arXiv:1511.08039.

[44] LHCb collaboration, R. Aaij *et al.*, *Measurement of the forward $Z$ boson production cross-section in pp collisions at $\sqrt{s}$ = 7 TeV*, JHEP **08** (2015) 039, arXiv:1505.07024.

[45] L. Anderlini *et al.*, *The PIDCalib package*, LHCb-PUB-2016-021, 2016.

[46] B. Efron, *Bootstrap methods: Another look at the jackknife*, The Annals of Statistics **7** (1979) 1 .

[47] A. Andreassen *et al.*, *OmniFold: A method to simultaneously unfold all observables*, Phys. Rev. Lett. **124** (2020) 182001, arXiv:1911.09107.

[48] G. D'Agostini, *A multidimensional unfolding method based on Bayes' theorem*, Nucl. Instrum. Meth. **A** (1995) 487.

[49] T. Adye, *Unfolding algorithms and tests using RooUnfold*, in *PHYSTAT 2011*, (Geneva), 313–318, CERN, 2011, arXiv:1105.1160.

[50] LHCb collaboration, R. Aaij *et al.*, *Measurement of forward $W$ and $Z$ boson production in association with jets in proton-proton collisions at $\sqrt{s}$ =8 TeV*, JHEP **05** (2016) 131, arXiv:1605.00951.

[51] Y. I. Azimov, Y. L. Dokshitzer, V. A. Khoze, and S. I. Troyan, *Humpbacked QCD plateau in hadron spectra*, Z. Phys. C **31** (1986) 213.